the FEBS Journal

The three-dimensional structure of VIM-31 – a metallo-β-lactamase from *Enterobacter cloacae* in its native and oxidized form

Michaël B. Kupper[1,*], Konrad Herzog[1,*], Sandra Bennink[1], Philipp Schlömer[1], Pierre Bogaerts[2], Youri Glupczynski[2], Rainer Fischer[1], Carine Bebrone[1] and Kurt M. Hoffmann[1]

1 Institute of Molecular Biotechnology, RWTH-Aachen University, Germany
2 Laboratory of Bacteriology, CHU Mont-Godinne-Dinant, Université Catholique de Louvain, Yvoir, Belgium

Keywords
active site; antibiotic resistance; crystallographic structures; *Enterobacter cloacae*; metallo-β-lactamase

Correspondence
K. Hoffmann and C. Bebrone, Institute of Molecular Biotechnology, RWTH-Aachen University, c/o Fraunhofer IME, Forckenbeckstraße 6, 52074 Aachen, Germany; Symbiose Biomaterials, Avenue de l'Hôpital 1, B34 (+3), 4000 Liège, Belgium
Fax: +49 241 6085 10000; +32 4 3664198
Tel: +49 241 6085 12032; +32 4 2427780
E-mails: kurt.hoffmann@rwth-aachen.de; carine.bebrone@symbiosebiomaterials.be
Website: http://www.symbiosebiomaterials.be

*These authors contributed equally to this work.

(Received 17 February 2015, revised 24 March 2015, accepted 25 March 2015)

doi:10.1111/febs.13283

The metallo-β-lactamase VIM-31 differs from VIM-2 by only two Tyr224-His and His252Arg substitutions. Located close to the active site, the Tyr224His substitution is also present in VIM-1, VIM-4, VIM-7 and VIM-12. The VIM-31 variant was reported in 2012 from *Enterobacter cloacae* and kinetically characterized. It exhibits globally lower catalytic efficiencies than VIM-2. In the present study, we report the three-dimensional structures of VIM-31 in its native (reduced) and oxidized forms. The so-called 'flapping-loop' (loop 1) and loop 3 of VIM-31 were not positioned as in VIM-2 but instead were closer to the active site as in VIM-4, resulting in a narrower active site in VIM-31. Also, the presence of His224 in VIM-31 disrupts hydrogen-bonding networks close to the active site. Moreover, a third zinc-binding site, which also exists in VIM-2 structures, could be identified as a structural explanation for the decreased activity of VIM-MBLs at high zinc concentrations.

Introduction

The emergence of metallo-β-lactamases (MBLs) becomes an increasingly important problem with respect to public health because these enzymes hydrolyze most of the commonly used β-lactam antibiotics, including expanded-spectrum cephalosporins and carbapenems [1]. Moreover, there is currently no clinically available inhibitor for MBLs [1]. MBLs are characterized by the presence of a common αββα fold [2] and require one or two zinc ions for their activity [1]. MBLs are divided into three subclasses (B1, B2 and B3) on the basis of sequence alignments [3,4].

The fact that some B1 MBL genes (notably those for VIM-1, IMP-1, NDM-1 and their variants) are plasmid-encoded represents an additional cause of

Abbreviations
DLS, dynamic light scattering; MBL, metallo-β-lactamase; PDB, Protein Data Bank; TCEP, Tris(2-carboxyethyl)phosphine.

concern [5]. Indeed, VIM-type B1 MBLs are among the most widespread and clinically relevant carbapenemases [6]. To date, 45 distinct bla_{VIM} alleles have been described from a variety of Gram-negative opportunistic pathogens (http://www.lahey.org/studies/other.asp#table1). The VIM family can be divided into three sublineages, VIM-1 [7], VIM-2 [8] and VIM-7 [9,10], based on their amino acid sequences. To date, the three-dimensional structures of representatives of each sublineage, VIM-4 and VIM-26 (which differ from VIM-1 by a single residue mutation, Ser228Arg and His224Leu, respectively), as well as VIM-2 and VIM-7, have been reported in their native or oxidized forms or in complex with inhibitor [11–15].

The VIM-31 enzyme was described in 2012 in an *Enterobacter cloacae* isolate from a patient hospitalized in Brussels (Belgium). VIM-31 differs from VIM-2 by only two mutations (Tyr224His and His252Arg according to the class B standard numbering) [4]. This Tyr224His substitution is also present in VIM-1 [7], VIM-4 [14], VIM-7 [9], VIM-12 [16], VIM-14 [17], VIM-19 [18] and VIM-27 [19]. VIM-31 exhibits globally lower catalytic efficiencies than VIM-2 (because of lower k_{cat} and higher K_m values) [20].

In the present study, we report the three-dimensional structures of VIM-31 in its native and oxidized forms and discuss the role of the Tyr/His224 residue in the active sites of VIM enzymes. As highlighted previously [13], there is no clinically useful inhibitor of MBLs and studies of functional and structural properties are important for future inhibitor design.

Moreover, we report the presence of a third zinc-binding site formed at the interface of the two molecules in the crystal lattice that may be relevant to the observed inhibition of VIM-31 activity at elevated zinc concentrations.

Results and Discussion

Two different VIM-31 structures were obtained: VIM-31 with Cys221 oxidized into a cysteine sulfonate residue (VIM-31-Ox) and a native VIM-31 structure (VIM-31) resulting from the use of a reducing agent (1 mM TCEP) during the crystallization process. The structures have been solved to 1.88 Å (VIM-31-Ox) and 1.61 Å (VIM-31). The final models (VIM-31-Ox and VIM-31) were refined to low *R*-factors (14.8% and 14.7%) and R_{free} values (19.5% and 18.6%). The crystallographic and model statistics for the structures are summarized in Table 1.

Both structures of VIM-31 show 231 residues (Gly30-Arg313) and the typical αββα folding described for the MBLs (Fig. 1A).

Table 1. X-ray data collection and structure refinement. Numbers in parentheses indicate highest resolution shell statistics.

	VIM-31-Ox	VIM-31
Data collection and scaling statistics		
X-ray wavelength (Å)	1.5418	1.5418
Unit cell parameters		
a (Å)	67.02	64.60
b (Å)	80.13	74.39
c (Å)	77.64	78.72
α (°)	90.00	90.00
β (°)	91.71	90.00
γ (°)	90.00	90.00
Space group	I121	I222
Molecules/ asymmetric unit	2	1
Resolution range (Å)	40–1.86	54–1.61
Number of observations	128 440	120 068
Number of unique reflections	33 380	24 650
Overall completeness (%)	97.2 (81.9)	97.9 (87.5)
$I/\sigma(I)$	20.0 (7.7)	15.5 (3.5)
Multiplicity	3.8 (3.7)	4.9 (4.5)
R_{sym}	0.044 (0.157)	0.059 (0.404)
Refinement statistics		
Resolution range (Å)	40–1.88	54–1.61
Number of reflections	31 694	23 393
Number of atoms (non-hydrogen)	4081	2012
R_{work}	0.1475	0.1474
R_{free}	0.1948	0.1856
rmsd from ideal		
Bonds (Å)	0.0121	0.0158
Angles (°)	1.0775	1.3118

Comparison between both structures (oxidized and native) of VIM-31

The rmsd values for Cα atoms between both VIM-31 structures (oxidized and reduced) were 0.324 Å (VIM-31-Ox chain A/VIM-31) and 0.378 Å (VIM-31-Ox chain B/VIM-31) (Fig. 1A).

B1 MBLs have a cysteine residue (Cys221) as one of the metal ligands in the Zn2 site that is susceptible to oxidation [2]. In VIM-31-Ox, only Zn1 was present in the 'histidine' site (His116-His118-His196) (Fig. 1B) and Cys221 was clearly oxidized into a cysteine sulfonate residue (Ocs221), as already observed in the VIM-2 and VIM-7 structures [11,12].

The oxidation problem appears to be recurrent with VIM MBLs. The presence of the strongly oxidized cysteine (Ocs221) was already reported in detail [8]. To determine the step at which the structural study Cys221 became oxidized, ESI-MS analysis of samples

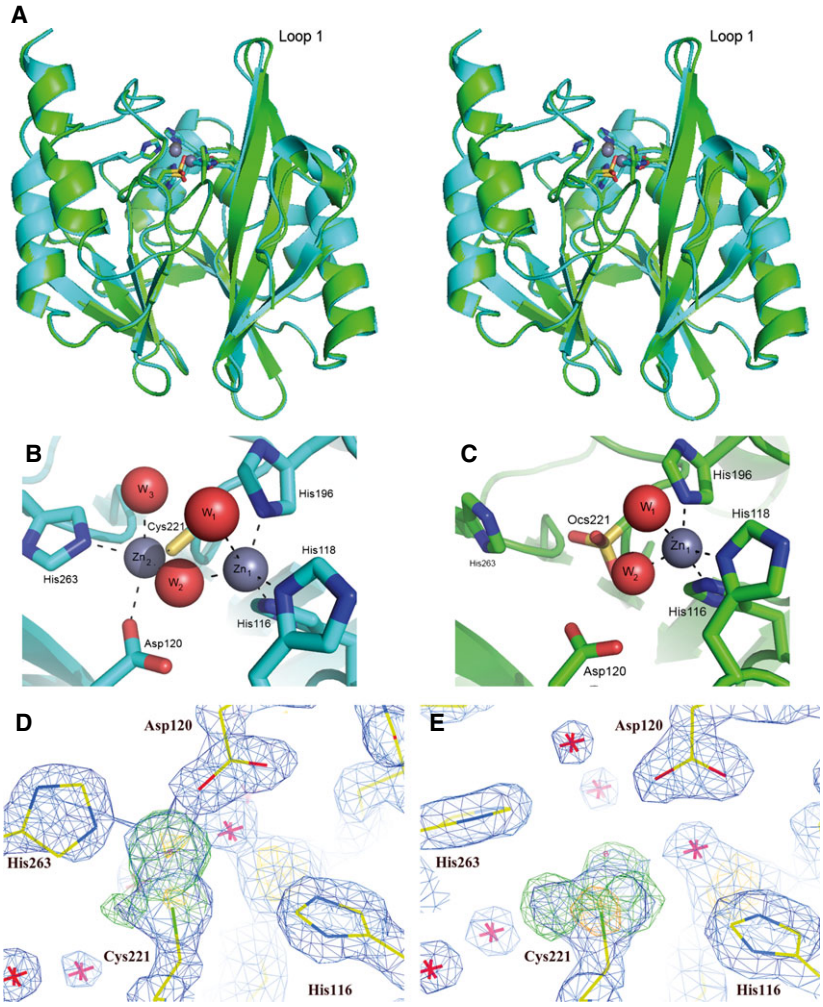

Fig. 1. (A) Stereoview of the structural superposition of reduced (native) VIM-31 (in cyan) and oxidized VIM-31 (in green). Residues of the active site are represented as sticks. (B) Zoom on the active site of the native form. The second zinc ion (Zn2) is bound in the 'cysteine' binding site. A water molecule (W2) bridges the two metal ions. A water molecule (W3) is the fifth ligand of Zn2. (C) Zoom on the active site of the oxidized form. The sole zinc ion (Zn1) is bound in the 'histidine' binding site. Two water molecules (W1 and W2) complete the coordination sphere of the zinc ion. Zinc ions and water molecules are represented as grey and red spheres, respectively. Electron density maps of Vim-31 (D) and VIM-31-Ox (E) active site. $2F_O - F_C$ map in blue (1.5σ), omit-map for Zn2 and Ocs221 side chain oxygen atoms in green (5.5σ) and anomalous difference map (4.0 σ) indicating zinc and sulfur in yellow.

of freshly-purified samples, or protein stored at −20 °C or after crystallization, was performed. It appears that oxidation most likely took place during the crystallization process. Only the presence of 1 mM TCEP or 8 mM β-mercaptoethanol prevented the oxidation process [11,12]. X-ray radiation damage during data collection was also ruled out because structures of VIM-2 obtained from synchrotron sources or from using the X-ray laboratory generator gave consistently the structure of oxidized VIM-2 [12]. Oxidized VIM-2 is an inactive enzyme [2].

On the other hand, a mono-zinc structure of VIM-4 that did not present an oxidation of Cys221 has been previously obtained [Protein Data Bank (PDB) code: 2WRS; P. Lassaux, unpublished results]. Within this non-oxidized mono-zinc structure, Zn1 was also bound in the 'histidine' site.

The active site of the reduced VIM-31 presents the two metal ion binding sites described for subclass B1 MBLs (the 'histidine' site and the 'cysteine' site, respectively) [2] (Fig. 1C). The two Zn ions (Zn1 and Zn2) are separated by 3.74 Å, a value similar to those observed for VIM-4 (3.8 Å/3.9 Å; PDB code: 2WHG), VIM-2 in complex with the rac-2-omega-phenylpropyl-3-mercaptopropionic acid inhibitor (3.8 Å/3.7 Å; PDB code: 2YZ3) and most other B1 MBLs, although significantly lower than the value observed for the native VIM-2 structure (4.2 Å; PDB code: 1KO3). The second Zn (Zn2) located in the 'cysteine' site has a lower occupancy than Zn1 (0.7). Indeed, despite the presence of 1 mM TCEP during the crystallization, the Cys221 residue is ~ 30% oxidized, which results in a 30% loss of Zn2. The reduced VIM-31 structure thus represents a mixture of the di-zinc (Cys221 bound to Zn2) (70%) and mono-zinc (Ocs221 and an empty Zn2 site) (30%) forms of the enzyme. The electron density maps depicted in Fig. 1(D–E) confirm the coexistence of an oxidized and a reduced Cys221 state

in VIM-31. Although, in VIM-31-Ox, Zn2 is completely absent and Cys221 is fully oxidized, in VIM-31, strong electron density and some weak anomalous density indicate the presence of Zn2. However, the existence of a population of oxidized Cys221 also can be observed from 'oxygen' electron density comparable to that of VIM-31-Ox.

As previously observed for the VIM-2 structures, the differences between the oxidized and the reduced forms of VIM-31 are mainly located in the second zinc-binding site (His263 and Asp120), the so-called 'flapping loop' (loop 1, 58–68) and Arg228. By contrast to the position of Tyr224, which was different in the oxidized VIM-2 in comparison with its reduced counterpart, the His224 residue occupies an identical position in the oxidized and reduced forms of VIM-31.

Comparison between the di-zinc structures of the VIM-31, VIM-2 and VIM-4 enzymes

VIM-31 differs from VIM-2 by two mutations (Tyr224His and His252Arg). VIM-31 and VIM-4 differ by 13 residues but have the His224 residue in common. The superposition of the VIM-31, VIM-2 and VIM-4 structures shows that they are closely related (Fig. 2A). Native VIM-31 has an overall RMSD for Cα atoms of 0.302 Å compared to VIM-2 (PDB code: 1KO3) and 0.301 Å compared to VIM-4 (PDB code: 2WHG, chain A).

In many B1 MBLs, residues 58–68 form a flexible surface loop (loop 1 or the so-called 'flapping loop') whose conformation varies in the available structures and can close over the active site upon substrate and inhibitor binding [1,2,21,22]. The 'flapping loop' of VIM-31 was not positioned as in VIM-2 but instead was closer to the active site as in VIM-4 (Fig. 2A).

For VIM-31 as for VIM-4, the Tyr224 residue present in VIM-2 is replaced by His224. The Tyr224His substitution occurs close to the active site and belongs to loop 3 (residues 223–242). Previous studies have proposed that, besides the conserved residues that participate in zinc coordination in MBLs, the active site is probably modulated by a hydrogen-bonding network of residues located along the sequence [23]. As already shown in VIM-7 [11], the presence of His224 in VIM-31 disrupts hydrogen-bonding networks close to the active site. In the VIM-2 crystal structure, the Tyr224 OH interacts with Gly232 N and, via a water molecule, with Asn233 O and with ND1 of the Zn1 ligand His196 [12] (Fig. 2B). In VIM-31, His224 is locked by Arg228 in a position, which prevents the interaction with this water molecule (Fig. 2C). However, in contrast to what has been observed in VIM-7 [11], the water molecule that connects Asn233 and the Zn1 ligand His196 is still present (Fig. 2C). Loss of

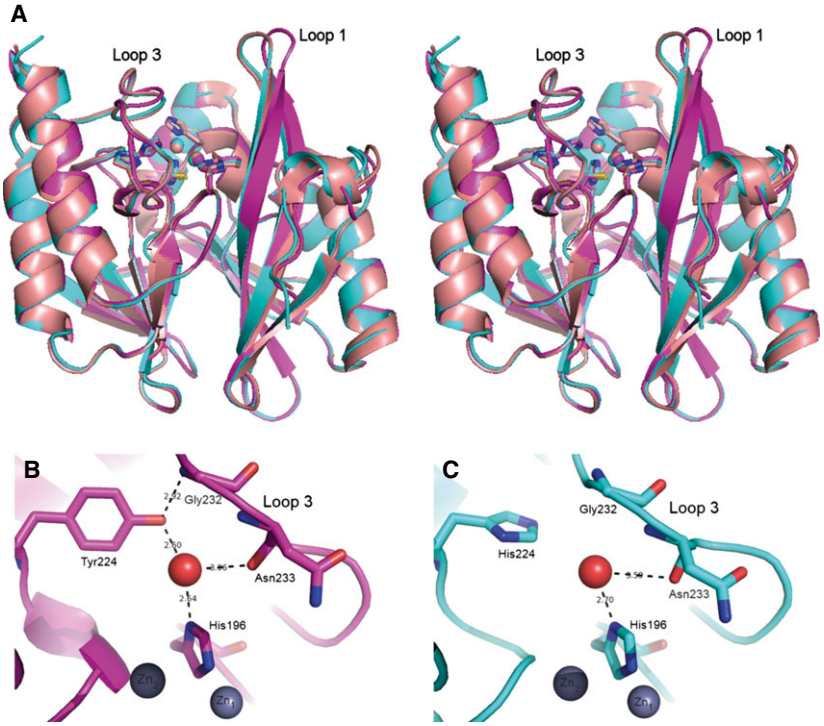

Fig. 2. (A) Stereoview of the overall structure comparison of VIM-31 (in cyan), VIM-2 (in magenta) and VIM-4 (in salmon). (B) Hydrogen-bonding network involving Tyr224 in VIM-2. (C) Loss of hydrogen-bonding contacts with the loop 3 region (Gly232-Asn233) as a result of the presence of His224 in VIM-31.

hydrogen-bonding contacts involving residues in the loop 3 region may possibly influence interactions with substrates and/or inhibitors because residues such as Arg228 and Asn233 are associated with substrate and inhibitor binding [12,22]. In VIM-31, the position of loop 3 and of the Arg228 and Asn233 residues is closer to that observed in VIM-4 than in VIM-2. Especially Arg228 appears to play an important role in binding the negatively-charged C3-substituting carboxyl group of β-lactam antibiotics. Several structures of the subclass B1 MBL NDM-1 have been solved in complex with different hydrolyzed β-lactam substrates [24], which, via the C3-carboxyl-group, interact with the conserved Lys224 residue. As already proposed for VIM-2 [12] and VIM-4 [14], Arg228 with its long side chain may replace Lys224 and interact with the carboxylate of β-lactams. As shown in Fig. 4, the Tyr224-His mutation from VIM-2 to VIM-31 strongly influences the conformation of Arg228. Compared to Tyr224, His224 forms a hydrogen bond with the arginine guanidine group. The resulting decrease in flexibility reduces the structural variability of the active site and might explain the lower catalytic efficiencies of VIM-31 and VIM-4 compared to VIM-2.

As a result of the respective positions of loops 1 and 3 closer to the active site, the binding cleft of VIM-31 is narrower than that of VIM-2 (Fig. 3). However, with the exception of cefoxitin (k_{cat}/K_m ratio for VIM-2/VIM-31 is 54), VIM-31 and VIM-2 exhibit similar kinetic behaviour [20]. Nevertheless, VIM-31 presents decreased K_m values compared to VIM-2 for benzylpenicillin, cefoxitin and ceftazidime (the K_m ratio for VIM-31/VIM-2 is > 3) (Table 2). VIM-31 presents decreased k_{cat} values for piperacillin, cefepime, cefoxitin, nitrocefin and meropenem (the k_{cat} ratio for VIM-2/VIM-31 is > 4) (Table 2). It should be noted that the comparison of the kinetic properties of VIM-31 to the VIM-2 variant was performed using previously determined data from Bogaerts *et al.* [20] and from Docquier *et al.* [8]. Because these experiments were performed by different groups in different laboratories, differences by factors of 2 or 3 should not be considered.

For both structures of VIM-31, a third zinc ion was found on the surface (Fig. 4). It is coordinated by His302 (2.06 Å from His ND1) from one molecule in the crystal and His166 (2.07 Å from His NE2) from a neighbouring molecule. Acetate ions complete the coordination sphere. Such a zinc ion is also found on the surface of both VIM-2 structures (PDB codes: 1KO3 and 1KO2), also bound to the His166 and His302 residues. Even if the zinc ion is not in close proximity to the active site, it can influence the shape

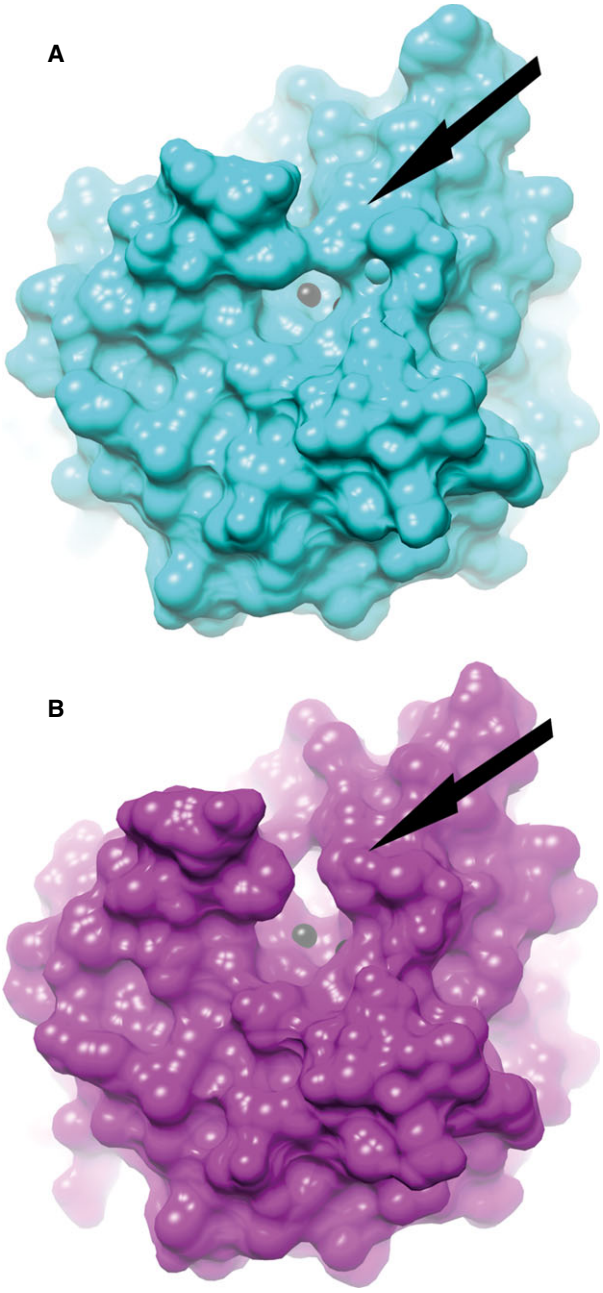

Fig. 3. Solvent-accessible surfaces. The active site is located at the bottom of a long groove running on the surface of the protein. The shape of the cleft is modulated by conformational changes of loops 1 and 3. An arrow indicates the active site cleft. (A) VIM-31. (B) VIM-2 (1KO3).

of the latter via a small hydrogen-bonding network between His302 and the backbone oxygens of loop 3. As discussed above, loop 3 is crucial for substrate binding in the active site. Inhibition of VIM-31 activity (as well as that of other VIM enzymes) [14] at zinc concentrations above 50 μM is observed. The position

Table 2. Comparison of kinetic parameters of VIM-31 and VIM-2 enzymes.

	VIM-31[a]			VIM-2[b]			
	k_{cat} (s^{-1})	K_m (μM)	k_{cat}/K_m ($mM^{-1}\cdot s^{-1}$)	k_{cat} (s^{-1})	K_m (μM)	k_{cat}/K_m ($mM^{-1}\cdot s^{-1}$)	k_{cat}/K_M ratio for VIM-2/VIM-31
Benzylpenicillin	108	270	400	280	70	4000	10
Piperacillin	66	72	920	300	125	2400	2.6
Ceftazidime	2.2	490	4.5	3.6	72	50	11
Cefepime	8.5	470	18	> 40	> 400	100	5.6
Cefoxitin	1.6	74	22	15	13	1200	54
Nitrocefin	152	35	4350	770	18	43 000	9.9
Meropenem	0.9	3	300	5	2	2500	8.3

[a]VIM-31 values reported by Bogaerts *et al.* [8].
[b]VIM-2 values reported by Docquier *et al.* [20].

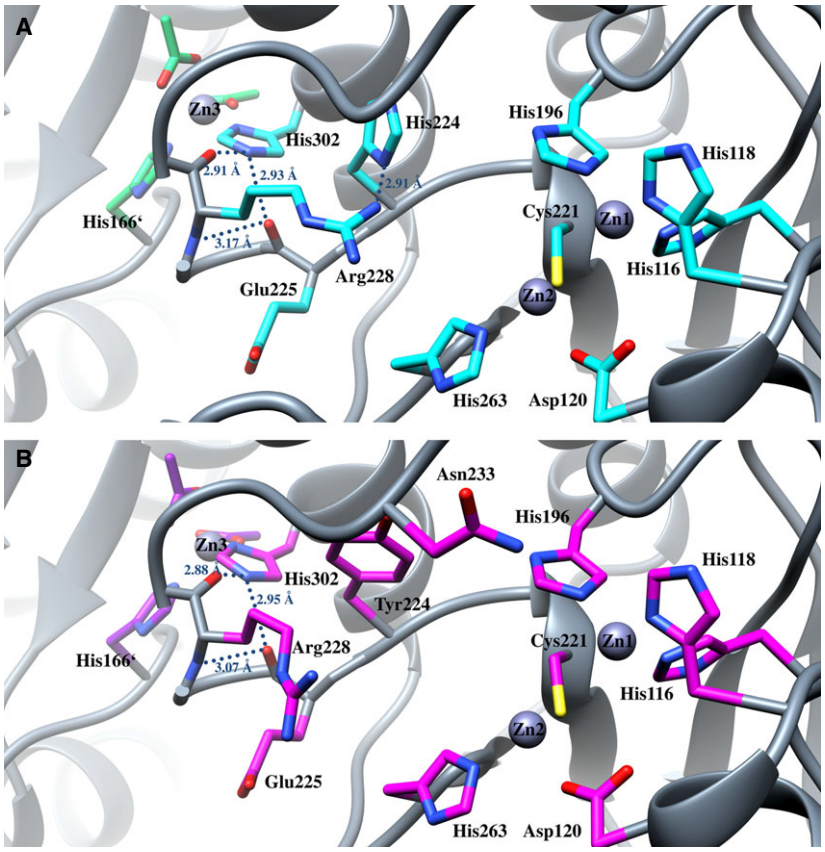

Fig. 4. Active site and loop 3 interactions of VIM-31 (A) and VIM-2 (B). His 166′ belongs to a neighbouring protein in the crystal. Blue dotted lines indicate the hydrogen bonds that could explain the zinc dependent activity of VIM-type MBLs on the basis of the third zinc-binding site on the protein surface. The hydrogen bonds are shown for (A) VIM-31: Glu225O-Arg228N (3.17 Å), Glu225O-His302NE2 (2.93 Å), His302NE2-Arg228O (2.91 Å), Arg228NH1-His224ND1 (2.91 Å) and (B) for VIM-2: Glu225O-Arg228N (3.07 Å), Glu225O-His302NE2 (2.95 Å), His302NE2-Arg228O (2.88 Å).

of the third zinc site, as well as its possible effect on the active site, could be one structural explanation for this zinc-dependent loss of activity. Furthermore, the association of VIM molecules via the zinc ion on the surface, as occurred during crystallization of VIM-2 and VIM-31, could reduce the concentration of dissolved active enzyme and thus provide an additional explanation for the zinc-dependent activity decrease described above. Dynamic light scattering (DLS) experiments with different Zn^{2+} concentrations show a strongly zinc-dependent aggregation of VIM-31 above 40 μM $ZnSO_4$ (Fig. 5). Even below this concentration, no monodisperse particle distributions with an apparent hydrodynamic radius in the range of 1–10 nm (as would be expected for a monodisperse protein solution) could be obtained. This phenomenon could be caused by the surface bound zinc ion described above, which is still present in a fraction of VIM-31 molecules, even after zinc removal by washing. Upon addition of zinc, aggregation takes place as shown by the increase of the hydrodynamic radii. At Zn^{2+} concentrations of 1280 μM and above, VIM-31

precipitates. Because aggregation/precipitation can lead to protein unfolding and thus to decreased enzymatic activity, the DLS results, in combination with the third zinc-binding site observed in VIM-31 and VIM-2 structures, provide a reasonable explanation for the zinc-dependent decrease of activity in VIM-type β-lactamases.

Conclusions

The so-called 'flapping-loop' (loop 1) and loop 3 of VIM-31, previously shown to be important for substrate binding, are not positioned as in VIM-2 but instead are closer to the active site as in VIM-4. This results in a narrower active site in VIM-31 and explains the globally lower affinities for β-lactams of this enzyme compared to VIM-2. The disruption of the hydrogen-bonding network close to the active site (involving the Zn1 ligand His196), as well as the flexibility reduction of Arg228 as a result of the presence of the His224 residue, could also have a negative effect on the catalytic efficiency of the enzyme. Finally, a third zinc-binding site, which also exists in VIM-2 structures, could be identified as providing a structural explanation for the decreased activity of VIM-MBLs at high zinc concentrations.

Materials and methods

Production and purification

The mature VIM-31 enzyme from *E. cloacae* was overexpressed in *Escherichia coli* BL21 (DE3) and purified as described previously [20].

Crystallization and structure solution

The initial crystals from VIM-31 (12 $mg \cdot mL^{-1}$ in 50 mM Hepes, pH 7.5, $ZnCl_2$ 50 μM) were obtained at 21 °C from 0.2 M lithium sulphate, 0.1 M Tris-HCl, pH 8.5, 30% poly (ethylene glycol) 4000, using the sitting drop method with crystallization plates designed by Taorad GmbH (Aachen, Germany). The reservoir solution (1 μL) was mixed with the protein solution (1 μL) and the mixture was left to equilibrate against the solution reservoir. Crystals appeared after 1 month; they belong to space group I121 with two molecules of VIM-31 in the asymmetric unit. Under these conditions, they showed oxidation of Cys221 (cysteinesulfonic form, Ocs221) (VIM-31-Ox). Crystals of the reduced form of VIM-31 (17 $mg \cdot mL^{-1}$ in 50 mM Hepes, pH 7.5, 50 μM $ZnCl_2$) were obtained under 0.3 M sodium acetate, 0.1 M Tris-HCl, pH 8.5, 20% poly(ethylene glycol) 4000 crystallization conditions with the addition of 1 mM of TCEP in the precipitant solution. Crystals appeared after ~ 1 month. They belong to space group I222 (VIM-31). For X-ray crystallography, the crystals were mounted directly without additional cryo-conditions and were flash-frozen at 100 K in a liquid nitrogen stream. The poly(ethylene glycol) concentration present in the crystallization conditions (20% and 30%, respectively) was sufficiently high to prevent ice ring formation and to preclude addition of supplementary cryo-protectant. Almost complete X-ray data sets were collected using a FR591 rotating anode X-ray generator (Bruker Instruments, Inc., Bellerica, MA, USA) and a Mar345dtb detector (marXperts GmbH, Norderstedt Germany). Test images were taken prior to data collection to determine the optimal detector position for good $I/\sigma(I)$-values of the highest resolution shell. Diffraction data were processed using IMOSFLM [25], analyzed regarding their symmetry using POINTLESS and scaled with SCALA [26] from the CCP4 software suite [27]. The structures of VIM-31 were solved by molecular replacement approach

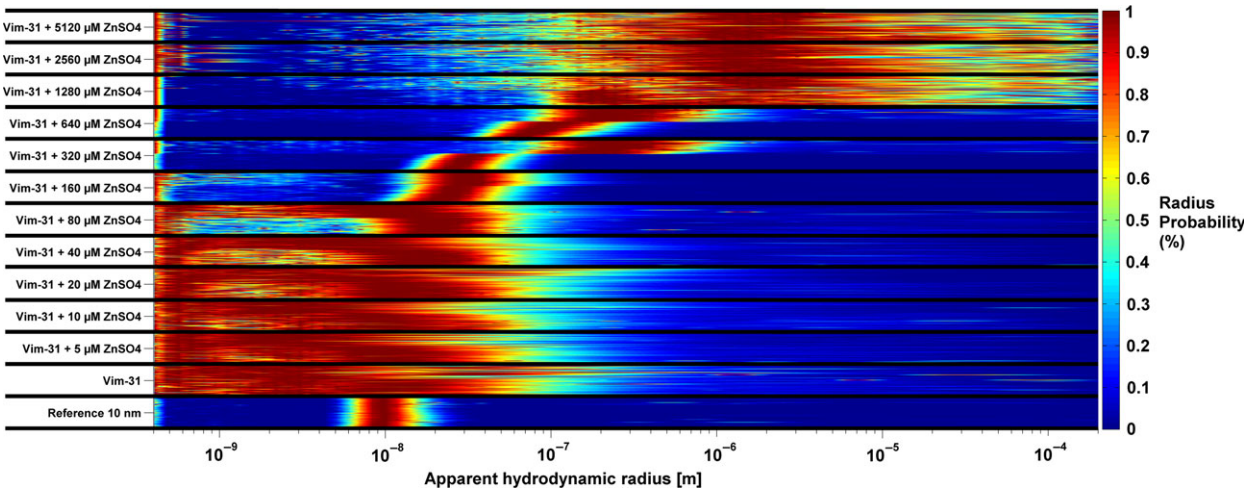

Fig. 5. DLS results of VIM-31 in the presence of different Zn^{2+}-concentrations. Each measurement-area with 84 data points covers a time span of 262 min, starting at the lower and ending at the upper border of the respective area.

using MOLREP [28] and the structure of VIM-2 (PDB code: 1KO3) [12] as a search model processed with CHAINSAW [29], both part of the CCP4 software suite. The structures were iteratively refined by manual inspection of the electron density with COOT [30] and refinement with REFMAC5 [31]. Refinement to convergence was carried out with isotropic B-values and using TLS parameters computed initially using the TLSMD server [32]. Alternative conformations were modelled for a number of side chains and occupancies were adjusted manually for some atoms. Occupancies for the different Cys221 oxidation states were adjusted iteratively according to B-factor analysis, anomalous scattering analysis and difference map analysis, until a satisfying agreement between structural model and observed X-ray data was achieved.

Accession codes

Coordinates and structure factors have been deposited in the PDB under accession codes 4FSB and 4FR7.

Zn^{2+} dependence of the VIM-31 activity

To determine the Zn^{2+} dependence of the VIM-31 activity, 1 mM benzylpenicillin was used as the substrate. Hydrolysis of this substrate was monitored by following the absorbance variations as described previously [20], using an Uvikon 943 spectrophotometer (NorthStar Scientific, Bardsey, UK) equipped with thermostatically controlled cells.

DLS

Measurements were carried out in 2-μL droplets under paraffin oil using glass-bottom plates by Taorad GmbH and an in-house developed laser light scattering device. For each droplet, 84 data points were collected within 264 min. VIM-31-$ZnSO_4$ solutions were prepared by mixing one part VIM-31 stock solution (20 $mg{\cdot}mL^{-1}$ protein in 20 mM Tris, pH 7.5) and one part $ZnSO_4$ stock solution (10, 20, 40, 80, 160, 320, 640, 1280, 2560, 5120 and 10 240 μM, respectively). Zinc free VIM-31 solution ($[Zn^{2+}] < 0.4$ μM) was prepared by repeated ultrafiltration and washing with 20 mM Tris, pH 7.5 (prepared with MilliQ water; Millipore, Billerica, MA, USA). Under these conditions, the VIM-31 enzyme was found by ESI-MS to bind two zinc ions per molecule of enzyme. Stock solutions were filtered (0.22 μm) before use. Latex beads (r = 10 nm) were used as a reference control. Data analysis was conducted in MATLAB (MathWorks, Inc., Natick, MA, USA).

Acknowledgements

The work in Aachen (Germany) was supported by the European Regional Development Fund (ERDF), the European Union ('Die Europäische Kommission investiert in Ihre Zukunft') and the Alma *in Silico* project financed by the Interreg IV Program. C. Bebrone was a fellow of the Alexander von Humboldt Foundation (Bonn, Germany).

Author contributions

CB, KMH, RF, PB and YG conceived and designed the experiments. MBK, KH, SB, PS and CB performed the experiments. CB, MBK, KH and KMH analyzed the data. PB and YG contributed reagents or other essential material. CB, MBK and KMH wrote the paper.

References

1 Bebrone C (2007) Metallo-β-lactamases (classification, activity, genetic organization, structure, zinc coordination) and their Superfamily. *Biochem Pharmacol* **74**, 1686–1701.
2 Bebrone C, Garau G, Garcia-Saez I, Chantalat L, Carfi A & Dideberg O (2012) X-ray structures and mechanisms of metallo-ß-lactamases, ß-lactamases. In: Molecular Anatomy and Physiology of Proteins, (Jean-Marie F, ed.), pp. 41–77. Nova Science Publishers, Hauppauge, NY, USA.
3 Galleni M, Lamotte-Brasseur J, Rossolini GM, Spencer J, Dideberg O & Frère JM (2001) Standard numbering scheme for class B beta-lactamases. *Antimicrob Agents Chemother* **45**, 660–663.
4 Garau G, Garcia-Saez I, Bebrone C, Anne C, Mercuri P, Galleni M, Frère JM & Dideberg O (2004) Update of the standard numbering scheme for class B β-lactamases. *Antimicrob Agents Chemother* **48**, 2347–2349.
5 Cornaglia G, Giamarellou H & Rossolini GM (2011) Metallo-β-lactamases: a last frontier for β-lactams?. *Lancet Infect Dis* **11**, 381–393.
6 Cantón R, Akóva M, Carmeli Y, Giske CG, Glupczynski Y, Gniadkowski M, Livermore DM, Miriagou V, Naas T, Rossolini GM *et al.* European Network on Carbapenemases (2012) Rapid evolution and spread of carbapenemases among Enterobacteriaceae in Europe. *Clin Microbiol Infect* **18**, 413–431.
7 Franceschini N, Caravelli B, Docquier JD, Galleni M, Frere JM, Amicosante G & Rossolini GM (2000) Purification and biochemical characterization of the VIM-1 metallo-beta-lactamase. *Antimicrob Agents Chemother* **44**, 3003–3007.
8 Docquier JD, Lamotte-Brasseur J, Galleni M, Amicosante G, Frère JM & Rossolini GM (2003) On functional and structural heterogeneity of VIM-type metallo-beta-lactamases. *J Antimicrob Chemother* **51**, 257–266.

9 Samuelsen Ø, Castanheira M, Walsh TR & Spencer J (2008) Kinetic characterization of VIM-7, a divergent member of the VIM metallo-beta-lactamase family. *Antimicrob Agents Chemother* **52**, 2905–2908.
10 Toleman MA, Rolston K, Jones RN & Walsh TR (2004) blaVIM-7, an evolutionarily distinct metallo-beta-lactamase gene in a *Pseudomonas aeruginosa* isolate from the United States. *Antimicrob Agents Chemother* **48**, 329–332.
11 Borra PS, Leiros HKS, Ahmad R, Spencer J, Leiros I, Walsh TR, Sundsfjord A & Samuelsen O (2011) Structural and Computational Investigations of VIM-7: insights into the Substrate Specificity of VIM Metallo-beta-Lactamases. *J Mol Biol* **411**, 174–189.
12 Garcia-Saez I, Docquier JD, Rossolini GM & Dideberg O (2008) The three-dimensional structure of VIM-2, a Zn-beta-lactamase from *Pseudomonas aeruginosa* in its reduced and oxidised form. *J Mol Biol* **375**, 604–611.
13 Leiros HK, Edvardsen KS, Bjerga GE & Samuelsen Ø (2015) Structural and biochemical characterization of VIM-26 show that Leu224 has implications for the substrate specificity of VIM metallo-ß-lactamases. *FEBS J* **282**, 1031–1042.
14 Lassaux P, Traoré DAK, Loisel E, Favier A, Docquier JD, Bebrone C, Frère JM, Ferrer JL & Galleni M (2011) Biochemical and structural characterisation of the subclass B1 metallo-β-lactamase VIM-4. *Antimicrob Agents Chemother* **55**, 1248–1255.
15 Yamaguchi Y, Jin W, Matsunaga K, Ikemizu S, Yamagata Y, Wachino J-I, Shibata N, Arakawa Y & Kurosaki H (2007) Crystallographic investigation of the inhibition mode of a VIM-2 metallo-beta-lactamase from *Pseudomonas aeruginosa* by a mercaptocarboxylate inhibitor. *J Med Chem* **50**, 6647–6653.
16 Kontou M, Pournaras S, Kristo I, Ikonomidis A, Maniatis AN & Stathopoulos C (2007) Molecular cloning and biochemical characterization of VIM-12, a novel hybrid VIM-1/VIM-2 metallo-beta-lactamase from a *Klebsiella pneumoniae* clinical isolate, reveal atypical substrate specificity. *Biochemistry* **46**, 13170–13178.
17 Mazzariol A, Mammina C, Koncan R, Di Gaetano V, Di Carlo P, Cipolla D, Corsello G & Cornaglia G (2011) A novel VIM-type metallo-beta-lactamase (VIM-14) in a *Pseudomonas aeruginosa* clinical isolate from a neonatal intensive care unit. *Clin Microbiol Infect* **17**, 722–724.
18 Rodriguez-Martinez JM, Nordmann P, Fortineau N & Poirel L (2010) VIM-19, a metallo-beta-lactamase with increased carbapenemase activity from *Escherichia coli* and *Klebsiella pneumoniae*. *Antimicrob Agents Chemother* **54**, 471–476.
19 Papagiannitsis CC, Kotsakis SD, Petinaki E, Vatopoulos AC, Tzelepi E, Miriagou V & Tzouvelekis LS (2011) Characterization of metallo-beta-lactamase VIM-27, an A57S mutant of VIM-1 associated with *Klebsiella pneumoniae* ST147. *Antimicrob Agents Chemother* **55**, 3570–3572.
20 Bogaerts P, Bebrone C, Huang T-D, Bouchahrouf W, De Gheldre Y, Deplano A, Hoffman K & Glupczynski Y (2012) Detection and characterization of VIM-31, a new variant of VIM-2 with Tyr224His and His252Arg mutations, in a clinical isolate of *Enterobacter cloacae*. *Antimicrob Agents Chemother* **56**, 3283–3287.
21 Garcia-Saez I, Hopkins J, Papamicael C, Franceschini N, Amicosante G, Rossolini GM, Galleni M, Frère JM & Dideberg O (2003) The 1.5 Å structure of *Chryseobacterium meningosepticum* zinc beta-lactamase in complex with the inhibitor, D-captopril. *J Biol Chem* **278**, 23868–23873.
22 Moali C, Anne C, Lamotte-Brasseur J, Groslambert S, Devreese B, Van Beeumen J, Galleni M & Frère JM (2003) Analysis of the importance of the metallo-beta-lactamase active site loop in substrate binding and catalysis. *Chem Biol* **10**, 319–329.
23 Murphy TA, Catto LE, Halford SE, Hadfield AT, Minor W, Walsh TR & Spencer J (2006) Crystal structure of *Pseudomonas aeruginosa* SPM-1 provides insights into variable zinc affinity of metallo-beta-lactamases. *J Mol Biol* **357**, 890–903.
24 King DT, Worrall LJ, Gruninger R & Strynadka NC (2012) New Delhi metallo-β-lactamase: structural insights into β-lactam recognition and inhibition. *J Am Chem Soc* **134**, 11362–11365.
25 Leslie AGW & Powell HR (2007) Processing diffraction data with Mosflm. *Evol Methods Macromol Crystallogr* **245**, 41–51.
26 Evans PR (2005) Scaling and assessment of data quality. *Acta Cryst* **D62**, 72–82.
27 Collaborative Computational Project, Number 4 (1994) The CCP4 suite: programs for protein crystallography. *Acta Cryst* **D50**, 760–763.
28 Vagin A & Teplyakov A (1997) MOLREP: an automated program for molecular replacement. *J Appl Cryst* **30**, 1022–1025.
29 Stein N (2008) CHAINSAW: a program for mutating pdb files used as templates in molecular replacement. *J Appl Cryst* **41**, 641–643.
30 Emsley P & Cowtan K (2004) Coot: model-building tools for molecular graphics. *Acta Crystallogr* **D60**, 2126–2132.
31 Murshudov GN, Skubak P, Lebedev AA, Pannu NS, Steiner RA, Nicholls RA, Winn MD, Long F & Vagin AA (2011) REFMAC5 for the refinement of macromolecular crystal structures. *Acta Crystallogr D* **67**, 355–367.
32 Painter J & Merritt EA (2006) TLSMD web server for the generation of multi-group TLS models. *J Appl Cryst* **39**, 109–111.